Editor's Choice

Electrophoresis of neutral oil in water

Volker Knecht [a,*], Zachary A. Levine [b], P. Thomas Vernier [b]

[a] Max Planck Institute of Colloids and Interfaces, Science Park Golm, 14424 Potsdam, Germany
[b] University of Southern California, Marina del Rey, USA

ABSTRACT

Negative electrophoretic mobilities of oil in water are widely interpreted in terms of adsorption of hydroxide leading to negative surface charge. Challenging this traditional view, an increasing body of evidence suggests surface depletion of hydroxide and surface accumulation of hydronium leading to a positive surface charge. We present results from molecular dynamics (MD) simulations showing electrophoretic mobilities of oil in water with the same sign and magnitude as in experiment but in the absence of ions. The underlying mechanism involves interfacial roughness leading to gradients in dielectric permittivity in field direction and, thus, local elevation of the applied electric field. Although all molecules have zero net charge, their partial charges are distributed non-uniformly such that oil exhibits negative and water positive excess charge in regions of high field intensities; this induces a net force on the oil or the water against or in field direction, respectively. Our results indicate that deducing net charges from electrophoretic mobilities as widely done can be misleading. Our findings suggest that pH dependent electrophoretic mobilities in experiment being negative above and positive below pH 2.5 arise from a competition between the negative mobility of the ion-free interface and the positive mobility from adsorbed hydronium ions.

© 2010 Elsevier Inc. All rights reserved.

1. Introduction

It has been known for two centuries [1] that a suspended particle exposed to a homogeneous static electric field may start to migrate, an effect denoted as electrophoresis. The drift velocity is proportional to the applied field. In general, the electrophoretic mobility, i.e., the migration rate normalized by the field intensity, is assumed to be proportional to the net charge on the particle. Based on this assumption, electrophoresis experiments are widely used to determine the charge of colloidal particles [2]. Oil droplets show electrophoretic mobilities that are negative above and positive below pH 2.5, denoted as isoelectric point (iep) [3,4]. This behavior is commonly explained in terms of adsorption of hydroxide (OH^-) or hydronium (H_3O^+) giving rise to a negative or positive surface charge depending on the pH [5,6]. Hydroxide adsorption at water/hydrophobe interfaces has been also inferred from measurements of disjoining pressures for thin water films as a measure for the interaction between the two interfaces of the film [5,7]. Furthermore, strong surface activity for hydroxide has been invoked to explain titration experiments on oil-in-water emulsions. Here it is observed that upon increasing the interfacial area by homogenization of the emulsion, a base needs to be added to maintain the apparent pH in the water.

The titration experiments rely on the measurement of the pH of an inhomogeneous oil-in-water emulsion. From the relatively large oil fraction used in these experiments, 2 vol.%, possible interference of the oil with the pH sensor counterfeiting the measurements cannot be excluded. In contrast, substantially lower oil fractions (e.g., 0.05 vol.% in studies by Marinova et al. [6]) are used in electrophoresis experiments, which thus may not suffer from this problem. The disjoining pressure measurements interpreted in terms of hydroxide adsorption require the presence of surfactants. Therefore, those measurements do not probe the bare but only the surfactant-covered aqueous interface.

Indeed, whereas titration, disjoining pressure, and electrophoresis studies are widely interpreted in terms of higher interfacial affinity for hydroxide than for hydronium, other investigations suggest that hydroxide might in fact be less surface active than hydronium if not even repelled from interfaces. Surface repulsion of hydroxide is suggested from surface tension measurements [8,9], second harmonic generation spectroscopy [10], and synchrotron photoelectron spectroscopy of NaOH in aqueous microjets [9]. Vibrational sum frequency generation spectra indicate strong surface enhancement of hydronium for strong acid solutions but no sign of surface enhancement of hydroxide for equally strong base solutions [11]. Classical MD simulations using polarizable force fields indicate that water/hydrophobe interfaces repel hydroxide and attract hydronium [11–13]. If hydronium exhibits higher or lower surface affinity than hydroxide and if the hydroxide

* Corresponding author. Fax: +49 331 567 9612.
E-mail address: vknecht@mpikg.mpg.de (V. Knecht).

concentration at interfaces is enhanced or reduced compared to the bulk water is a matter of ongoing debate [9,10,14–20].

Recent MD simulations showed negative electrophoretic mobilities of oil in water although ions were absent but the underlying mechanism remained unclear [21]. Later this effect was observed to depend on the treatment of the dispersion interactions using Lennard-Jones (LJ) potentials. Electrophoretic drift was observed when the LJ interactions were truncated abruptly such that the force was discontinuous at the cut-off distance and when a cut-off distance of 1 nm was chosen. When the LJ interactions were modified such that the force smoothly reached zero at the cut-off boundary or the cut-off distance was increased to 2 nm, the electrophoretic drift vanished [22].

The simulations in [21,22] used a simplified description where hydrogens of CH_n groups were treated implicitly using compound atoms and molecules were non-polarizable. Here we show that for a more detailed model in which not only the water but also CH_n groups are described in full atomic detail and molecules are polarizable, uncharged oil in water may show electrophoretic drift even for continuous LJ forces. The electrophoretic mobility of the oil is of the same sign and size as the mobilities of oil droplets in distilled water measured experimentally. The mechanism underlying the electrophoretic drift in our simulations is revealed. In particular, we also show why this effect is not observed for the simplified description. Our findings suggest that electrophoretic mobility does not always reflect the charge of an oil droplet. Our results render the negative electrophoretic mobilities of oil droplets in water consistent with a small positive surface charge indicated from the results from the spectroscopic experiments and the MD simulations.

2. Methods and theory

2.1. Simulation setup

The system mainly considered in this work is shown in Fig. 1 and specified as system DEC in Table 1. It consisted of a decane slab in water parallel to the xy plane under periodic boundary conditions. An initial configuration for this system as well as the force field parameters and the simulation protocol as used in [13] were provided by Vacha. Hence, the initial configuration of a larger slab denoted as system DECL was modeled as a 2×2 array of the configuration of DEC. In addition, a cubic box of bulk water or bulk water containing a single methane denoted as system WAT or MET, respectively, in Table 1, were simulated. System DEC was simulated at equilibrium and exposed to external fields in the

Table 1
The systems simulated consisted of a decane slab in water of two different sizes denoted as DEC and DECL, pure bulk water (WAT), and bulk water containing a single methane molecule (MET). Given are the number of decane ($N_{sys,a}$) or water molecules ($N_{sys,w}$), and the initial size of the simulation box, $a \times b \times c$.

| System	$N_{sys,a}$	$N_{sys,w}$	$a \times b \times c$ (nm³)
DEC	64	723	$2.5 \times 2.5 \times 7.3$
DECL	256	2892	$5.0 \times 5.0 \times 7.3$
WAT	–	461	$2.8 \times 2.8 \times 2.8$
MET	–	457	$2.8 \times 2.8 \times 2.8$

range $E_0 = 0.05–0.5$ V/nm in x direction. Here, for system DEC at equilibrium and for each out of four different field intensities, a single 10 ns simulation was conducted. For this system, in addition, thirty 1.6 ns simulations at equilibrium and different field intensities were started from the same initial configuration but different sets of initial velocities. Likewise, for system DECL, thirty 200 ps simulations at $E_0 = 0.5$ V/nm were started from the same initial configuration but different sets of initial velocities. System WAT and MET were each simulated for 4 ns at equilibrium.

The decane was described using a polarizable potential derived from the general Amber force field (GAFF) [23]. The force field for the methane (CH_4) molecule was derived from that for a CH_3 group by adapting the partial charges for the hydrogens keeping them as close as possible to the values for CH_3 but yielding a zero net charge for CH_4. The water was described using the polarizable POL3 water model [24,25] in conjunction with the SETTLE algorithm to keep the O–H and H–H distances at ideal values. Polarizability was simulated by using the shell model of Dick and Overhauser [26]. Here, a shell particle representing the electronic degrees of freedom is attached to a nucleus by a spring and the potential energy is minimized with respect to the shell position every step. Lennard Jones (LJ) interactions were treated unchanged for interatomic distances r with $0 < r < r_1 = 0.7$ nm; for $r_1 < r < r_c = 1$ nm, a third degree polynomial $S(r)$ denoted as switch function was added to the force such that the modified force and its derivative were continuous at $r = r_1$ and $r = r_c$ [27].

The neighbor list for non-bonded interactions considering all pairs of atoms separated by less than 1.1 nm was updated every 10 steps. Full electrostatic interactions were considered using the particle mesh Ewald (PME) technique [28] using tinfoil boundary conditions [29] with (i) a cut-off distance of 1.1 nm in direct space and (ii) a 0.12 nm grid spacing and a 4th order polynomial for interpolation for the reciprocal sum. Decane and water were separately coupled to an external temperature bath of 300 K using a Berendsen thermostat [30] with a relaxation time of 0.1 ps. For systems DEC or DECL the pressure in xy direction and for systems WAT or MET the pressure in all directions were coupled to 1 bar using a Berendsen barostat [30] with a coupling constant of 1 ps. All simulations were performed using GROMACS [31], version 3.3.1. The simulations required 40500 CPU hours on AMD Opteron 3.0 GHz dual processor/dual core nodes. Configurations were saved every 5 ps for further analysis.

For system DECL at an external field of 0.5 V/nm, thirty 200 ps simulations were started from the same initial configuration but different sets of initial velocities using modified LJ interactions with $r_1 = 1.7$ nm and $r_c = 2$ nm and modified electrostatic interactions with a cut-off distance of 2.1 nm in direct space. For comparison to previous studies of oil slabs in water, an additional 100 ns simulation at an external field of 0.5 V/nm was carried out using a non-polarizable force field. Here, the (non-polar) hydrogen atoms of the decane molecules were described using united atoms using the GROMOS-87 force field [32] and the water was treated using the three-site simple point charge (SPC) model [33]. All other conditions were kept identical to the other setup.
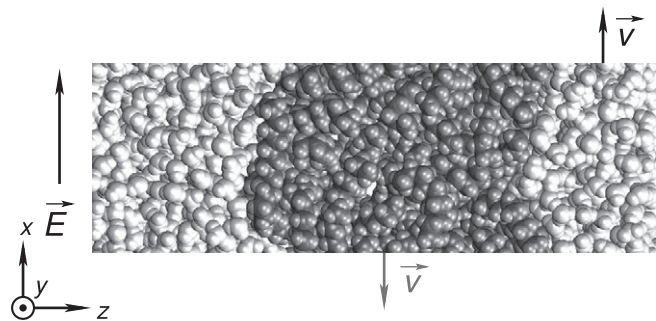
Fig. 1. The system simulated was a decane slab in water in the absence of ions. The system was described with an all-atom polarizable force field and LJ forces were smoothed at the cut-off distance. An electric field applied parallel to the water/decane interface induces a tangential movement between the phases; the decane phase migrates against and the water in field direction. The water is shown in white and the decane in gray. The figure was prepared using VMD [39].

2.2. Analysis of water/decane system

2.2.1. Electrophoretic motion

Analyses of the systems at equilibrium or at steady states were performed omitting the initial 100 ps for relaxation. If not stated otherwise, standard errors were obtained from block averages dividing the trajectories into four fragments. For system DEC or DECL, the central observable was the position $\mathbf{r} = (x,y)$ of the center of mass of the decane slab relative to the center of mass of the water parallel to the interface (xy plane). Here we distinguished between the position in field direction, x, and normal to the field direction, y. For each field intensity, migration rates $v \equiv \Delta x/\Delta t$ and corresponding standard errors were determined from the initial and final configurations of the sampling period of the thirty 1.6 ns simulations for system DEC and the thirty 200 ps simulations for system DECL. For migration rates from the 10 ns simulations of the polarizable all-atom and the non-polarizable united atom model at $E_0 = 0.5$ V/nm, standard errors were obtained by dividing the trajectory into four segments. Electrophoretic mobilities were obtained from fitting the function $v = \mu_E E_{app}$ to the data from the thirty 1.6 ns simulations of system DEC, with the effective electric field E_{app} taken equal to the electric field in the water bulk. The latter was determined from [34]

$$E_{app} = \frac{np}{(\epsilon_w - 1)\epsilon_0}. \tag{1}$$

Here, p is the average dipole moment of a water molecule in field direction in the water phase at least 1 nm away from the Gibbs dividing surface (position at which the water density equals half the density in the water bulk). Furthermore, $n = 33/\text{nm}^3$ is the bulk number density of the water molecules and ϵ_0 is the permittivity of vacuum. The value $\epsilon_w = 122$ for the relative permittivity of POL3 was obtained from the fluctuations of the dipole moment $\mathbf{M}$ of a box of water (system WAT) according to [34]

$$\epsilon_w = 1 + \frac{1}{3\epsilon_0} \frac{\langle \mathbf{M}^2 \rangle}{V k_B T} \tag{2}$$

Here, V is the volume of the box, k_B Boltzmann's constant, $T = 300$ K the temperature, and $\langle \ldots \rangle$ denotes an average over the simulation. The spatial flow pattern was studied by comparing the average velocity v_{loc} of atoms with the mass density ρ of the system both as a function of the position z normal to the interface at an effective field of 0.2 V/nm. The bin widths chosen for the distance scale where 0.6 nm for v_{loc} and 0.018 nm for ρ.

2.2.2. Drive versus friction

To dissect drive and friction governing electrophoretic motion in our system, the flow of matter normal to the interface is considered to undergo a discontinuous transition at the interface. If E_{app} is the applied electric field and F the force driving electrophoretic movement, the quantity $Q \equiv F/E_{app}$ has units of a charge and is denoted as *pseudo charge*. If A_i is the interfacial area, the quantity $\sigma \equiv Q/A_i$ is denoted as surface pseudo charge. The friction force is given by $F_R = b A_i \Delta v$ where $\Delta v = v/2$ and b denotes the friction coefficient [35]. At steady state, $F = F_R$, yielding

$$\mu_E = 2\sigma/b. \tag{3}$$

The friction coefficient was determined from the mobility $\mu \equiv v/F$ of the decane slab according to

$$b = \frac{2}{\mu A_i}, \tag{4}$$

where $A_i = 2A_b$ with A_b being the average area of the box parallel to the interface (xy plane). The mobility was obtained via the Einstein relation

$$\mu = \frac{D}{k_B T} \tag{5}$$

where D denotes the diffusion constant. The latter was evaluated from the thermal movement between the decane and the water slab parallel to the interface in the 10 ns simulations by subtracting the drift along x as follows. From the quantity $\tilde{\mathbf{r}}(t) = (x(t) - vt, y(t))$, the mean square displacement, defined as

$$\text{msd}(t) = \langle [\tilde{\mathbf{r}}(t' + t) - \tilde{\mathbf{r}}(t')]^2 \rangle_{t'} \tag{6}$$

was determined. Here $\langle \cdots \rangle_{t'}$ denotes an average over the times t'. Error bars for $\text{msd}(t)$ give the standard error from estimates from the simulations at different field strengths. The diffusion constant is determined from $D = \text{msd}(t_0)/t_0 2d$ with $t_0 = 400$ ps and $d = 2$ denoting the dimension of space. The pseudo charge density is determined from

$$\sigma = \frac{1}{A_i} \frac{\mu_E}{\mu} \tag{7}$$

Standard errors for μ_E, σ and b are obtained from the standard errors for migration rates v and mean square displacements $\text{msd}(t)$ via error propagation.

2.2.3. Equilibrium properties

Equilibrium properties for a water/decane interface were determined from the 10 ns simulation of system DEC omitting the initial 100 ps for equilibration. As a measure for the linear extension of a decane molecule, the quantity $d = 2r_g$ with r_g denoting the radius of gyration of a decane molecule defined by

$$r_g = \left(\frac{\sum_i \|\mathbf{r}_i\|^2 m_i}{\sum_i m_i} \right)^{\frac{1}{2}} \tag{8}$$

was determined by averaging over all decane molecules. Here, m_i denotes the mass of atom i and $\mathbf{r}_i$ the position of atom i with respect to the center of the molecule. Furthermore, the average surface area of the decane phase was analyzed. Here, the total "solvent accessible" surface area (SASA) of a given water/decane configuration, denoted as A_s, was determined. The SASA is defined as the area traced out by the center of a probe sphere representing a water molecule as it is rolled over respective groups of the solute and was calculated based on an algorithm by Connolly [36] using the program g_sas from the GROMACS suite [31]. The SASA per projected interfacial area, a, was obtained from $a = A_s/A_i$. For each configuration, the number of contacts between decane carbons and water oxygens considering all carbon–oxygen pairs separated by less than 0.5 nm, and the respective time average, N_{CO}, were calculated. The number of contacts per unit area, c_0, was obtained from

$$c_0 = N_{CO}/A_i. \tag{9}$$

The mass densities of water or oil, ρ_w or ρ_a, respectively, were determined as a function of the position z normal to the interface choosing a bin width of 0.018 nm and smoothed using a Gaussian filter with a width of 0.073 nm. Hence, the respective normalized densities

$$\chi_i = \rho_i/\rho_{i,b}, \quad i = w, a, \tag{10}$$

were evaluated. Here, $\rho_{i,b}$ denotes the mass densities in the bulk of the respective phase. The charge density $q_a(z)$ of the oil was obtained from

$$q_a(z) = \left\langle \sum_{i;|z_i - z| < \Delta z/2} q_i/A_b \Delta z \right\rangle. \tag{11}$$

Here, $\sum$ is a sum over respective atoms or shell particles of the oil, z_i denotes the position of atom i normal to the interface, q_i is the

partial charge of the atom or shell particle i, $\Delta z = 0.0061$ nm, and $q_a(z)$ was smoothed using a Gaussian filter of 0.0244 nm width.

2.3. Analysis of methane/water system

For each configuration of the single methane molecule in water (system MET), the number of contacts between the methane carbon and water oxygens considering pairs with a separation less than 0.5 nm was determined, and the respective time average, N_w, was calculated. The number density of water oxygens, n_O, and the number density of water hydrogens divided by two, n_H, was determined as a function of the distance r from the center of mass of the methane molecule. In addition, the number density of water oxygens n_{OO} as a function of the distance from the center of mass of a water molecule, averaged over all water molecules, was evaluated. The charge density $q_w(r)$ of the water was obtained from

$$q_w(r) = \langle \sum_{i:|r_i - r| < \Delta r/2} q_i / 4\pi r^2 \Delta r \rangle. \tag{12}$$

Here, $\sum$ is a sum over respective atoms or shell particles of the water, r_i denotes the value of r for atom or shell particle i, $\Delta r = 0.003$ nm, and $q_w(r)$ was smoothed with a Gaussian filter of 0.012 nm width. The dielectric permittivity in the methane molecule, ϵ_m, was determined from the fluctuations of the dipole moment $\mathbf{M}_w$ of the methane molecule according to [37]

$$\epsilon_m = 4\epsilon_w / \left(\frac{1}{\epsilon_0(2\epsilon_w + 1)} \frac{\langle \mathbf{M}_w^2 \rangle}{3V_m k_B T} - 1 \right). \tag{13}$$

Here, the volume of the methane molecule, V_m, was determined from $V_m = (4\pi/3)r_m^3$ with $r_m = d_{OC} - 0.5\ d_{OO}$ where d_{CO} or d_{OO} denote the position of the first maximum of $n_O(r)$ or $n_{OO}(r)$, respectively. The value for the dielectric permittivity of the water, $\epsilon_w = 122$, was determined as described above using Eq. (2). The value for the permittivity obtained was $\epsilon_m = 9.4 \pm 0.2$.

The electrostatics for a single methane molecule in water exposed to an electric field was analyzed using a corresponding spatially dependent dielectric permittivity $\epsilon(\mathbf{r})$ derived from the MD simulations. Hence, the component of the local electric field $E(\mathbf{r})$ in the direction of an applied field was evaluated from continuum electrostatics. The dielectric permittivity $\epsilon(r)$ as a function of the distance from the center of mass of the methane molecule, r, was determined by fitting a smoothed step function

$$\epsilon(r) = \epsilon_m + \frac{\epsilon_w}{\exp(-(r - r_0)/\Delta r) + 1} \tag{14}$$

to the normalized water density

$$\tilde{\chi}(r) \equiv \left(\frac{n_O(r) n_H(r)}{n_{O,b} n_{H,b}} \right)^{\frac{1}{2}}. \tag{15}$$

Here, $n_{O,b}$ or $n_{H,b}$ denote the respective values of $n_O(r)$ or $n_H(r)$ in the bulk. The fit yielded $r_0 = 0.311$ nm and $\Delta r = 0.0088$ nm.

This dielectric function was used to model the methane molecule in water for the continuum calculations. Here, the electric conductivity of 5.5E-6 S/m and the dielectric constant 122 for the bulk water were chosen. The function Eq. (14) specified the dielectric constant within a sphere of radius 1.0 nm. This sphere was embedded at the center of a cylinder of length 30 nm and a radius of 3 nm. The planar surfaces of the cylinder were chosen to differ in electrostatic potential such as to obtain an electric field $E_w = 20$ V/cm in the high dielectric region. This field strength is in the range of the field strengths used in electrophoresis experiments [6]. The Poisson equation for this system was solved numerically via the finite element method using the electrostatics module of the software COMSOL [38]. Here, a large number of 'mesh' volume elements are created and Poisson's

equation is solved individually for each element matching the boundary conditions specified. Inside the sphere, the COMSOL parameter 'maximum element size' was set to 1.0E-10 whereas the maximum element size in water (outside the sphere) was set to 1.0E-4.

Hence, using cylindrical symmetry, the local electric field E parallel to x emerging in response to the applied field was calculated as a function of the position along the axis, x, and the distance from the axis, ρ. This yielded the normalized field

$$\alpha(\rho, x) = E(\rho, x)/E_w \tag{16}$$

on the defined mesh. One-dimensional profiles $\alpha(0, x)$ and $\alpha(\rho, 0)$ with bin sizes 0.001 nm were determined via interpolation and smoothed with a rectangular filter of 0.04 nm width.

2.3.1. Mean-field calculation of electrophoretic pseudo charge

Although the total charge of water or oil is zero each, a non-zero force on the water or oil may result from a nonuniform distribution of respective partial charges leading to excess charge $q_i(\mathbf{r})$ with $i = w,a$ for water or oil, respectively, with sign and magnitude depending on the position $\mathbf{r}$. An electric field E_{app} parallel to the interface will result in a position dependent local electric field denoted as $E(\mathbf{r})$ due to gradients in dielectric permittivities. This will lead to a net force $F_{mf,i} = \int E(\mathbf{r}) q_i(\mathbf{r}) d^3\mathbf{r}$ on the water or the oil, corresponding to a pseudo charge $Q_{mf,i} = F_{mf,i}/E_{app}$. This pseudo charge was estimated from a mean-field description. The pseudo surface charge of water is calculated using the pseudo charge of the hydration shell of the single methane molecule in water, Q_w given by $Q_w = F_w/E_w$; here, F_w denotes the total force on the hydration shell in the presence of an external field of intensity E_w in the bulk water corresponding to a high dielectric environment. Q_w was determined from (i) the charge distribution $q_w(r)$ evaluated via Eq. (12), and (ii) the electric field normalized to the field in the water bulk, $\alpha(\rho, x)$, obtained as described in Section 2.3, according to

$$Q_w = 2\pi \int_0^w q_w((\rho^2 + x^2)^{1/2}) \alpha(\rho, x) \rho \, d\rho \, dx. \tag{17}$$

Here, $w = 1.18$ nm, and the integral was evaluated as a sum with the integrand and respective volume elements calculated on a regular grid with bin size 0.001 nm for ρ and x. To this aim, the profiles $q_w((\rho^2 + x^2)^{1/2})$ from Eq. (12) and $\alpha(\rho, x)$ from Eq. (16) defined on other grids were interpolated accordingly.

If an external field is applied parallel to a water/decane interface, the average electric field is the same in the bulk of the water and in the oil phase as known from continuum electrostatics. Hence, the average electric field is independent of the position z normal to the interface; its value is denoted as E_{app} as used in Eq. (1). At a particular z position at the interface, both water and oil molecules are present, and E_{app} arises from an average over contributions from the respective water and the oil fraction. If $\chi_w(z)$ or $\chi_a(z)$ denote the water or the oil fraction with $\chi_w(z) + \chi_a(z) = 1$ and $E_w(z)$ or $E_a(z)$ are the respective intensities of the electric field, the relation

$$E_{app} = \chi_w(z) E_w(z) + \chi_a E_a(z) \tag{18}$$

holds. We write

$$E_a(z) = \alpha_m E_w(z). \tag{19}$$

Here, α_m denotes an effective factor by which the electric field in the oil is enhanced compared to the electric field in the water fraction. A range of values for this factor was estimated as described based on findings from the analysis in Section 2.3 as described in the Results section. With $\chi(z) \equiv \chi_w(z)$ and $\chi_a(z) = 1 - \chi(z)$ we obtain

$$E_w(z) = \frac{E_{app}}{\chi(z) + \alpha_m - \alpha_m \chi(z)}. \tag{20}$$

Here we determine $\chi(z)$ from the number density of water oxygens along z, $n_w(z)$, and the respective density in the bulk water, $n_{w,b}$, according to $\chi(z) = n_O(z)/n_{O,b}(z)$. The contribution of the water at position z to the total pseudo charge of the interfacial water will scale with the respective number of atomic contacts between water and oil per unit volume, $c(z)$, estimated from

$$c(z) = a\chi(z)(1 - \chi(z)). \qquad (21)$$

Here, a is chosen such that $\int_{-u}^{+u} c(z)dz = c_0$, with c_0 denoting the number of oxygen–carbon contacts per unit interfacial area as obtained from Eq. (9), and $u = 1.8$ nm. If Q_w denotes the pseudo charge on the hydration shell of a methane molecule determined from Eq. (17), N_w denotes the number of interatomic contacts between water and methane analyzed as described above, and

$$\tilde{q}_w(z) \equiv \frac{Q_w}{N_w} c(z), \qquad (22)$$

the electrophoretic force $F_{w,i}$ on the water at a water/decane interface with projected interfacial area A_b is

$$F_{w,i} = A_b \int_{-u}^{+u} E_w(z)\tilde{q}_w(z)dz. \qquad (23)$$

The surface pseudo charge of the water is $\sigma_w = F_{w,i}/E_{app}A_b$. Using Eq. (20) we obtain

$$\sigma_w = \frac{Q_w}{N_w} \int_{-u}^{+u} \frac{c(z)}{\chi(z) + \alpha_m - \alpha_m\chi(z)} dz. \qquad (24)$$

The surface pseudo charge on the oil, σ_a is defined by

$$\sigma_a = F_{a,i}/E_{app}A_b, \qquad (25)$$

where $F_{w,i}$ denotes the electrophoretic force on the decane at a water/decane interface with projected interfacial area A_b. The surface pseudo charge on the oil obeys

$$\sigma_a = \frac{\int_{-u}^{+u} q_a(z)E_a(z)dz}{E_{app}}. \qquad (26)$$

Eqs. (18) and (19) yield

$$E_a(z) = \frac{E_{app}}{1 - \chi(z) + \frac{\chi(z)}{\alpha_m}}. \qquad (27)$$

Hence, the surface pseudo charge on the oil is obtained from

$$\sigma_a = \int_{-u}^{+u} \frac{q_a(z)}{1 - \chi(z) + \frac{\chi(z)}{\alpha_m}} dz. \qquad (28)$$

3. Results and discussion

3.1. Polarizable oil in water exhibits negative electrophoretic mobilities

The system simulated is shown in Fig. 1 and consisted of a decane ($C_{10}H_{22}$) slab in water under periodic boundary conditions. The decane was described using a polarizable potential derived from the general Amber force field (GAFF), and the water was treated using the polarizable POL3 water model [24,25]. The surface tension of the water/decane interface in the simulations at zero field intensity was 43 ± 8 mN/m, and, hence, within the error equal to the experimental value of 50.11 ± 0.04 mN/m, giving confidence that the model gives a reliable description of the interface.

To compare with previous studies [21,22], simulations in which decane was described using the GROMOS-87 force field [32] and the water was treated using the simple point charge (SPC) model [33] were carried out as well. LJ interactions were switched between 0.7 and 1.1 nm. An electric field of 0.28 V/nm was applied parallel to the decane slab and the average drift v of decane relative

to water in field direction was measured. As given in Table 2, the drift vanished for SPC/GROMOS but was non-zero for POL3/GAFF. Increasing the size of the oil slab or increasing the cut-off distance to 2 nm for POL3/GAFF did not affect the drift velocities significantly. In the following we will focus on the results from simulations using POL3/GAFF.

Fig. 2a shows that the data are consistent with a linear scaling of v with the field intensity, indicating electrophoretic motion. A linear fit yields an electrophoretic mobility of $-1.21 \pm 0.04 \times 10^{-8}$ m^2/Vs as given in Table 3. This is of the same sign and similar magnitude as electrophoretic mobilities in the range -2 to -5.5×10^{-8} m^2/Vs for micron-sized oil droplets in distilled water measured experimentally [3]. The electrophoretic mobilities, as well as other properties of a water/oil interfaces given below, are summarized in Table 3.
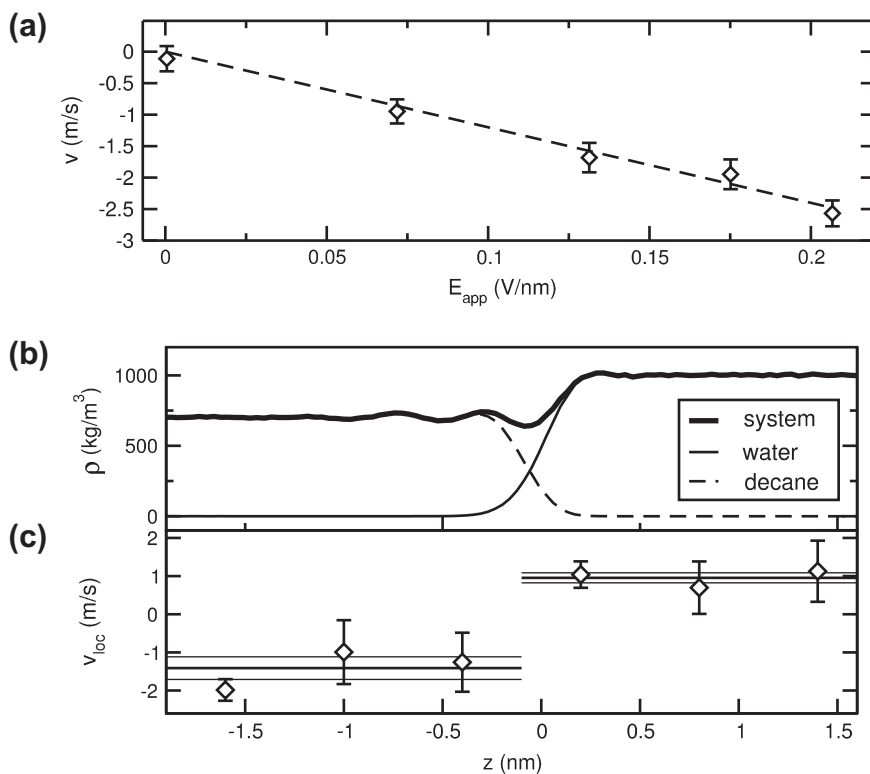
Fig. 2 b and c shows steady state properties for a water/decane interface parallel to an effective field of 0.21 V/nm. The mass densities of decane, water, and the total system (Fig. 2b) and the average velocity v_{loc} in field direction (Fig. 2c) are plotted as a function of the position z normal to the interface. The data suggest that $v_{loc}(z)$ is constant in the bulk phases and exhibits a transition at the interface. Thus, the interface is subjected to shear forces. Note that the transition in $v_{loc}(z)$ occurs within a distance range of 0.6 nm. For comparison, the effective linear size of a decane molecule, $d = 2r_g$, given by its radius of gyration, r_g, is found to be 0.7 nm. The length scale over which $v_{loc}(z)$ changes from the value in the oil to that in the water phase is thus comparable or even smaller than the molecular dimensions.

The current theory describes the flow profile $v(z)$ as a continuous transition using continuum hydrodynamics. In general, continuum theory is appropriate for processes whose typical length scales in the system are large compared to the molecular dimensions which is not the case here. Although continuum theory has been successfully used in explaining the mobilities of ions in water [40] or the hydrodynamic properties of proteins based on detailed models for the macromolecular surfaces [41], it is not clear a priori if continuum theory would be suitable for the process considered here. Hence, instead of describing $v(z)$ as a continuous transition using continuum hydrodynamics, we approximate the flow profile as a discontinuous transition associated with a friction coefficient b. The friction coefficient is determined from the thermal motion of decane parallel to water yielding $b = (0.74 \pm 0.02) \times 10^6$ Pa m s. This is similar to the coefficient of $b = 0.7 \times 10^6$ Pa m s for the friction between the two leaflets of a fluid lipid bilayer from previous MD simulations [42]. The driving force normalized by the field intensity shall be denoted as electrophoretic pseudo charge [21]. The pseudo charge normalized by the projected interfacial area is the surface pseudo charge σ. The surface pseudo charge is related to the friction coefficient and the electrophoretic mobility according to Eq. (3). We obtain $\sigma = -0.028 \pm 0.001$ e/nm^2.

Table 2
Electric field induced drift of decane slabs in water in molecular dynamics simulations. The initial projected area of the decane slab, A_b(nm^2), the force field, the cut-off distance for van der Waals interactions, r_{vdw}, and the migration rate in the direction of an external electric field of 0.5 V/nm parallel to the interface, v, are given. The two different values for A_b correspond to the systems DEC or DECL given in Table 1. The interaction potentials used were the non-polarizable united atom GROMOS/SPC and the polarizable all-atom GAFF/POL3 force field. Van der Waals interactions were switched between $r_{vdw} - 0.3$ nm and r_{vdw}. The drift is zero for GROMOS/SPC and non-zero for GAFF/POL3.

A_b (nm^2)	Force field	r_{vdw} (nm)	v (m/s)
6.25	GROMOS/SPC	1	-0.1 ± 0.2
6.25	GAFF/POL3	1	-3.6 ± 0.2
25.00	GAFF/POL3	1	-4.2 ± 0.3
25.00	GAFF/POL3	2.0	-4.1 ± 0.5

Fig. 2. Electrophoresis of uncharged decane in water. (a) Migration rate v of decane in water as a function of the applied electric field, E_{app}. The data set and a fit of the function $v = \mu_E E_{app}$ are shown. (b and c) Steady state properties for water/decane interface parallel to an effective electric field of 0.20 V/nm with (b) mass densities and (c) average velocity in field direction as a function of the position normal to the interface. In (c), horizontal lines indicate the average velocity in the respective bulk phase and the respective standard errors.

Table 3
Parameters for water/oil interfaces from MD simulation at finite ($E \neq 0$) or zero field intensities ($E = 0$) as well as from experiment. The electrophoretic mobility, μ_E, the friction coefficient for tangential movement between the phases, b, the electrophoretic pseudo charge, σ, and the isoelectric point, pI, are given.

Quantity	MD, $E \neq 0$	MD, $E = 0$	Experiment
$\mu_E(10^{-8}$ m^2/Vs)	-1.21 ± 0.04	-0.3 to -1.5	-2 to -5.5 [3]
b (10^6 Pa s)	0.74 ± 0.02	0.8 ± 0.1	–
σ (e/nm^2)	-0.028 ± 0.001	-0.008 to -0.037	–
pI	2.50 ± 0.04	2.4 to 3.0	2.5 [4]

### 3.2. Mechanism for charge-free electrophoresis

The electrophoretic mobility of a particle in an electrolyte solution can be affected by ion relaxation and polarization of the double layer and could be even non-zero for a particle with zero net charge but finite quadrupole moment [43–45]. However, a theory explaining the finite electrophoretic mobility of neutral oil in water in the absence of an electrolyte as observed here is not available. The physical mechanism underlying this phenomenon will be revealed in this section. Analysis shows that the water accessible surface area of the oil is 2.9 times larger than the projected interfacial area. This indicates considerable interfacial roughness and solvent exposure of hydrophobic groups. The number of contacts between water molecules and CH$_n$ groups per projected interfacial area is $36.3(\pm 0.07)$/nm$^2 \equiv c_0$. For comparison, we find that the first hydration shell of a single methane (CH$_4$) molecule in water with an outer shell diameter of 1.3 nm contains 16.8 ± 0.1 water molecules. The structure of this hydration shell will give rise to an electrophoretic pseudo charge as shown in the following.

Fig. 3 shows the density of water oxygens and hydrogens (a) and the excess charge $q_w(r)$ from the water (b) as a function of the distance r from the center of mass of the methane molecule at equilibrium. The distance at which the water density equals half the density in the bulk is indicated with a dotted line. This distance corresponds to a spherical shell which we shall denote as the dividing surface between methane and water. The water oxygens and hydrogens exhibiting negative or positive partial charges, respectively, are distributed unequally, leading to positive excess charge close to methane where the water density is low. Here, the dielectric permittivity, ϵ_m, is lower than in the bulk water, ϵ_w. Analysis of the dipole fluctuations yields $\epsilon_w = 122$ from Eq. (2) and $\epsilon_m = 9.4$ from Eq. (13).

The dielectric permittivity at the interface between methane and water between the two bulk values was interpolated according to Eq. (14). Hence, the electrostatics around a methane molecule in water placed at the origin and exposed to an external field in x direction was evaluated using continuum theory. The corresponding position dependent electric field normalized by the electric field denoted as α as a function of x and the distance from the x axis, ρ, is shown in Fig. 4. In the methane molecule, $\alpha = 1.54$. Normal to the direction of the applied field, α monotonically decreases to one for increasing distance r from the center of the methane molecule. Parallel to the applied field there is a minimum at the dividing surface ($r = 0.32$ nm).

Thus, positive excess charge of the water resides in a region where the electric field is enhanced compared to the water bulk. On the contrary, negative excess charge of the water partially resides in a region where the electric field is decreased compared to the water bulk. Thus, although the hydration shell has a total charge of zero, the total force on the water, being the spatial integral over the local excess charge times the local electric field as expressed in Eq. (17), will be positive. The pseudo charge of the hydration shell obtained from Eq. (17) is $Q_w = 0.8$ e.
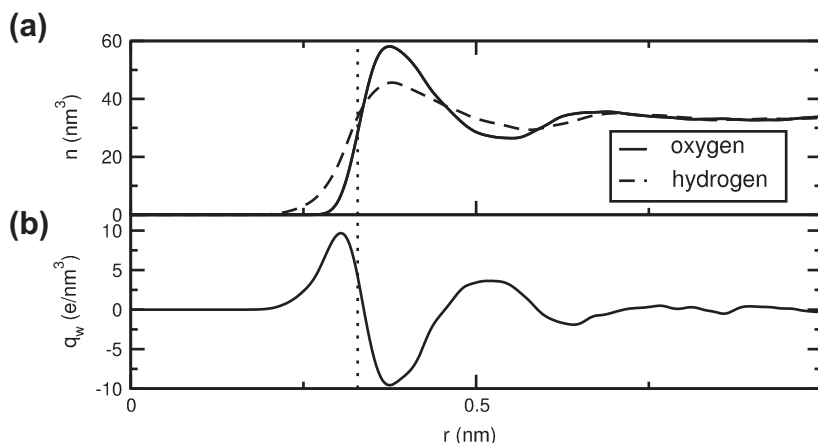
Fig. 3. Equilibrium properties of a single methane molecule in water. (a) The number densities of water oxygens or hydrogens and (b) the charge density from the water are shown as a function of the distance from the center of mass of the methane molecule.
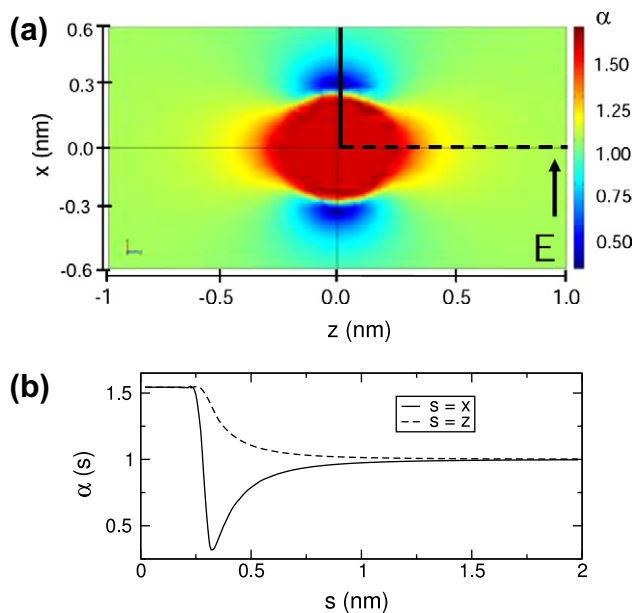
Fig. 4. Electrostatics for single methane molecule in water exposed to an electric field in the x direction. The ratio of the local electric field over the intensity of the field in the water bulk, α, is shown. (a) Two-dimensional representation. Here, the methane molecule is centered at the origin, the direction of the electric field is depicted, and α at each position (x,z) is color-coded. The system is cylindrically symmetric around the x axis. (b) α along the solid and the dotted lines in (a).

Hence, the surface pseudo charge for the water at a water/decane interface can be estimated from Eq. (24). The missing parameter here is α_m denoting the effective factor by which on average the electric field in the oil is enhanced compared to the bulk water. Here we assume that the electrostatics around the methyl(ene) groups from the decane exposed to interfacial water is locally similar to the electrostatics for the methane molecule in water. Fig. 4 shows that the electric field in the water is not constant but the methane affects the electric field beyond the dividing surface over a distance comparable to the radius of the methane molecule. Parallel to the applied field, as noted above, the electric field shows a local minimum corresponding to $\alpha = 0.29 \equiv \alpha_{min}$ at the dividing surface. At the water/oil interface, the water region around interfacial methyl(ene) groups will not be as extended as for the single methane molecule in water; hence, the electric field will most likely not reach its asymptotic value corresponding to $\alpha = 1$. Thus

the average electric field in the water will correspond to an average α-value denoted as α_{eff} between 0.29 and 1. The effective factor α_m will thus lie in the range between $\alpha_m/1$ and α_m/α_{min}. Hence,

$$1.54 < \alpha_m < 5.32. \tag{29}$$

This yields a surface pseudo charge for the water at a water/decane interface in the range between 30 and 60 e/nm^2.

A negative surface pseudo charge on decane in water is revealed from the properties of a water/decane interface at equilibrium shown in Fig. 5. The figure shows (a) the densities of water or decane normalized to the respective densities in the bulk phases, and (b) the excess charge per unit volume of the oil. It is evident that the oil exhibits negative excess charge in the region of low oil density at $z > 0$. In this region, the local electric field in the oil phase is larger than for $z < 0$ for the following reason. The electric field parallel to the interface, E, will be the same in the water and in the oil phase as known from continuum electrostatics, hence $E(z) = $ const $\equiv E_{app}$. Microscopically, $E(z)$ arises from an average over the electric field $E_w(z)$ in the water and $E_a(z)$ in the oil fraction according to Eq. (18). The corresponding surface pseudo charge of the oil can be obtained from Eqs. (28) and (29), yielding -0.018 e/nm$^2 < \sigma_a < -0.004$ e/nm^2.

The force on the oil phase in the presence of an electric field E_{app} will be $F_a = \sigma_a A_b E_{app}$, where A_b denotes the projected interfacial area (area of the simulation box in xy direction). This will be opposite in sign but smaller in magnitude than the respective force on the water, $F_w = \sigma_w A_b E_{app}$. The latter may be written as $F_w = F_{w,rel} + F_{w,abs}$ with $F_{w,rel} \equiv -F_a$. The force $F_{w,abs}$ will act on the center of mass of the system. For our simulations the center of mass motion is removed while in experiment $F_{w,abs}$ is counterbalanced by an opposing force from the electrodes; hence $F_{w,abs}$ will not lead to motion in either case. In contrast, $F_{w,rel}$ and F_a will lead to a total force $F = F_a - F_{w,rel} = 2F_a$ acting on the oil relative to the water. With Eqs. (7) and (25) this yields

$$\sigma = 2\sigma_a, \tag{30}$$

resulting in -0.037 e/nm$^2 < \sigma < -0.008$ e/nm^2, as given in Table 3. This range includes the surface pseudo charge σ determined from the electrophoretic motion in the MD simulations.

When oil and water are treated using the SPC/GROMOS model, the structure of water close to CH$_n$ groups is similar to that observed here for CH$_4$ [21]. However, there is no partial charge on the oil, so the respective surface pseudo charge must be zero and the electrophoretic mobility μ_E will vanish. This is consistent with the absence of electrophoretic motion for water/oil interfaces
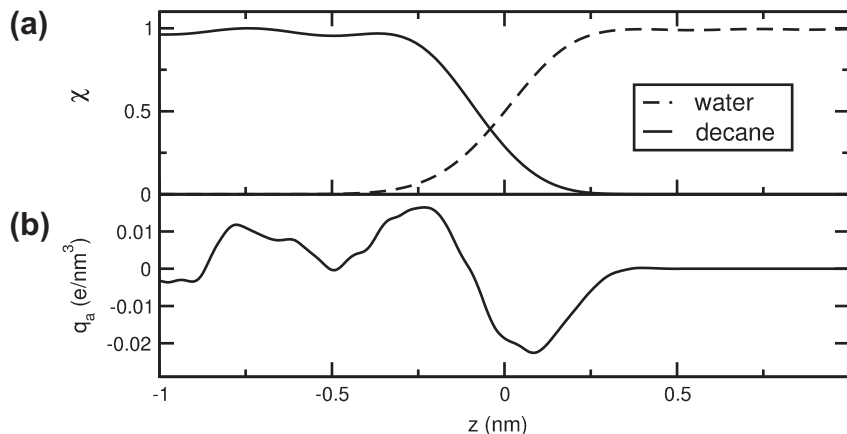
Fig. 5. Equilibrium properties of a water/decane interface. (a) The density of water or decane normalized to the respective bulk densities and (b) the excess charge density of the decane as a function of the position normal to the interface are depicted.

parallel to an applied electric field in this model observed here and by others [22].

3.3. Electrophoretic mobility reproduced from equilibrium properties

Due to the computational expense, only nm length scales and time scales of tens of nanoseconds are accessible with maintainable computational effort for the detailed model used here. To be able to distinguish electrophoretic motion from diffusion for this time and length scale, high electric fields in the range 0.05–0.15 V/nm were applied (the values refer to the value of the electric field in the water bulk). Although these exceed those typically used in electrophoresis experiments [6] by several orders of magnitude, the migration rates of the oil slabs observed in our simulations scale linear with the field intensity, indicating that nonlinear effects are not significant. This suggests that the simulations performed at high electric field intensities can be directly related to the available experimental data [21].

Moreover, we may predict the electrophoretic mobility for the oil slab considered here even solely from the equilibrium properties, that is, the properties at zero field strength. To this aim, we use (i) the friction coefficient as determined from an equilibrium simulation, and (ii) the surface pseudo charge from the mean-field calculations, σ_{mf}. We iterate that our mean-field model was parameterized based on results from an MD simulation at equilibrium and continuum calculations for an applied field using linear response theory. With $b = 0.8 \pm 0.1 \times 10^6$ Pa m s and the range for σ_{mf} from the mean-field theory as given in Table 3 we obtain -1.5×10^{-8} m^2/Vs $< \mu_E < -0.3 \times 10^{-8}$ m^2/Vs. This range includes the value for the electrophoretic mobility determined from the drift at non-zero field.

3.4. Role of ions

Experimental electrophoretic mobilities of oil droplets in water are pH dependent being negative for pH > pI and positive for pH < pI with pI denoting the isoelectric point (iep). The negative electrophoretic mobilities above the iep are commonly explained in therms of adsorption of hydroxide ions at the interface. However, findings from surface tension measurements and spectroscopic experiments as well as MD simulations indicate that hydrophobic surfaces in water repel hydroxide and attract hydronium [12–14]. For hydronium at a water/alkane interface an adsorption free energy of $\Delta G = -1.9$ kcal/mol is found from MD simulations [13]. Our results suggest that the positive surface charge from hydronium, $\sigma_+(pH)$, may compete with the negative

pseudo charge σ_a of the oil yielding the total surface charge, $\sigma(pH)$, according to

$$\sigma(pH)/2 = \sigma_a + \sigma_+(pH) \tag{31}$$

such that $\sigma(pH) < 0$ for pH > pI and $\sigma(pI) = 0$. Note that Eq. (31) is a generalization of Eq. (30). At pH 7, a hydronium or a hydroxide ion in solution would be present in a system of the size simulated for only 1.6×10^{-6} of the time. The number of hydronium ions $\Delta N(pH)$ adsorbed at an interface with a total area of ΔA is

$$\Delta N(pH) = 10^{-pH} \frac{mol}{L} \Delta z \Delta A \exp(-\Delta G/k_B T). \tag{32}$$

Here, k_B is Boltzmann's constant, $T = 300$ K the temperature, and Δz the thickness of the layer in which hydronium is adsorbed. Simulations suggest $\Delta z = 0.3$ nm [13]. With $\Delta A = 2A_b$, A_b being the average area of the box parallel to the interface as defined in Section 2.2.2 and pH = 7 we obtain $\Delta N \approx 5 \times 10^{-6}$. With

$$\sigma_+(pH) = e\Delta N(pH)/\Delta A \Delta z \tag{33}$$

and, hence, $\sigma_+(7) = 4 \times 10^{-7}$ e/nm^2, the total surface charge from Eq. (31) would be equal to the surface pseudo charge of the ion-free interface within the error. Consequently, within the statistical accuracy the electrophoretic mobility of decane, $\mu_E = 2\sigma/b$, would be the same as that of the ion-free interface. Hence, not to include any ions in our simulation system is a good approximation at neutral pH. Increasing the pH would not change the electrophoretic mobility significantly, in agreement with experiment [6]. At the iep, $\sigma(pI) = 0$, and, hence, $\sigma_+(pI) = -\sigma_a$. This yields

$$pI = -\frac{1}{\ln 10} \left[\frac{\Delta G}{k_B T} + \ln \left(\frac{-\sigma_a}{e} \frac{L}{mol} \right) \right] = 2.50 \pm 0.04. \tag{34}$$

This is in excellent agreement with the experimental value pI = 2.5 [4].

4. Conclusions

The current interpretation of electrophoresis experiments based on continuum theory relies on the assumption that, in general, electrophoretic mobility reflects net charge. Our MD simulations indicate that this assumption is invalid for oil droplets in water. A molecular mechanism for electrophoretic mobility of uncharged oil in water is revealed. Remarkably, we find that the negative electrophoretic mobilities of oil droplets in water are consistent with a small positive surface charge indicated from previous spectroscopic and simulation results.

Acknowledgments

References

[1] F. Reuss, Mém. Soc. Naturalistes Moscou 2 (1809) 327.
[2] R.J. Hunter, Zeta Potential in Colloid Science, Academic Press, London, 1981.
[3] M. Mooney, Phys. Rev. 23 (1924) 396.
[4] J.C. Carruthers, Trans. Faraday Soc. 34 (1938) 300.
[5] K.A. Karraker, C.J. Radke, Adv. Colloid Interface Sci. 96 (2002) 231.
[6] K.G. Marinova, R.G. Alargova, N.D. Denkov, O.D. Velev, D.N. Petsev, I.B. Ivanov, R.P. Borwankar, Langmuir 12 (1996) 2045.
[7] C. Stubenrauch, R. von Klitzing, J. Phys. – Condens. Matter 15 (2003) R1197.
[8] P. Weissenborn, R. Pugh, J. Colloid Interface Sci. 184 (1996) 550.
[9] B. Winter, M. Faubel, R. Vacha, P. Jungwirth, Chem. Phys. Lett. 474 (2009) 241.
[10] P.B. Petersen, R.J. Saykally, Chem. Phys. Lett. 458 (2008) 255.
[11] M. Mucha, T. Frigato, L. Levering, H. Allen, D. Tobias, L. Dang, P. Jungwirth, J. Phys. Chem. B 109 (2005) 7617.
[12] V. Buch, A. Milet, R. Vacha, P. Jungwirth, J.P. Devlin, Proc. Natl. Acad. Sci. U. S. A. 104 (2007) 7342.
[13] R. Vacha, D. Horinek, M.L. Berkowitz, P. Jungwirth, Phys. Chem. Chem. Phys. 10 (2008) 4975.
[14] R. Vacha, V. Buch, A. Milet, P. Devlin, P. Jungwirth, Phys. Chem. Chem. Phys. 9 (2007) 4736.
[15] J.K. Beattie, Phys. Chem. Chem. Phys. 10 (2008) 330.
[16] R. Vacha, V. Buch, A. Milet, J.P. Devlin, P. Jungwirth, Phys. Chem. Chem. Phys. 10 (2008) 332.
[17] J. Beattie, A. Djerdjev, G. Warr, Faraday Discuss. 141 (2009) 31.
[18] A. Gray-Weale, Chem. Phys. Lett. 481 (2009) 22.
[19] B. Winter, M. Faubel, R. Vacha, P. Jungwirth, Chem. Phys. Lett. 481 (2009) 19.
[20] R. Zimmermann, U. Freudenberg, R. Schweiß, D. Küttner, C. Werner, Curr. Opin. Colloid Interface Sci. 15 (2010) 196.
[21] V. Knecht, H.J. Risselada, A.E. Mark, S.J. Marrink, J. Colloid Interface Sci. 318 (2008) 477.
[22] D.J. Bonthuis, D. Horinek, L. Bocquet, R.R. Netz, Phys. Rev. Lett. (2009) 103.
[23] J. Wang, R. Wolf, J. Caldwell, P. Kollman, D. Case, J. Comput. Chem. 25 (2004) 1157.
[24] J. Caldwell, L. Dang, P. Kollman, J. Am. Chem. Soc. 112 (1990) 9144.
[25] J. Caldwell, P. Kollman, J. Phys. Chem. 99 (1995) 6208.
[26] B. Dick, A. Overhauser, Phys. Rev. 112 (1958) 90.
[27] D. van der Spoel, et al., GROMACS User Manual, version 3.3, 2006.
[28] T. Darden, D. York, L. Pedersen, J. Chem. Phys. 98 (1993) 10089.
[29] P. Hünenberger, in: L. Pratt, G. Hummer, (Eds.), Simulation and Theory of Electrostatic Interactions in Solution: Computational Chemistry, Biophysics, and Aqueous Solutions American Institute of Physics, 1999, pp. 17–83.
[30] H. Berendsen, J. Postma, W.F. van Gunsteren, A. Di Nola, J. Haak, J. Chem. Phys. 81 (1984) 3684.
[31] D. van der Spoel, E. Lindahl, B. Hess, G. Groenhof, A.E. Mark, H.J.C. Berendsen, J. Comput. Chem. 26 (2005) 1701.
[32] W.F. van Gunsteren, H.J.C. Berendsen, GROMOS-87 Manual, BIOMOS b.v., Nijenborgh 4, 9747 AG Groningen, The Netherlands, 1987.
[33] J. Hermans, H.J.C. Berendsen, W.F. van Gunsteren, J.P.M. Postma, Biopolymers 23 (1984) 1513.
[34] M. Neumann, Mol. Phys. 50 (1983) 841.
[35] W.K. den Otter, S.A. Shkulipa, Biophys. J. 93 (2007) 423.
[36] M.L. Connolly, Science 221 (1983) 709.
[37] V. Ballenegger, R. Blaak, J.P. Hansen, in: M. Ferrariao, G. Ciccotti, K. Binder, (Eds.), Conference on Computer Simulations in Condensed Matter Systems: From Materials to Chemical Biology, vol. 2, Erice, Italy, July, 2005, Lecture Notes in Physics, vol. 704, 2006, pp. 45–63, ISBN 978-3-540-35283-9.
[38] COMSOL multiphysics (version 3.4) (2007), <http://www.comsol.com/company/>.
[39] W. Humphrey, A. Dalke, K. Schulten, J. Mol. Graph. 14 (1996) 33.
[40] L. Onsager, R. Fuoss, J. Phys. Chem. 36 (1932) 2689.
[41] J. de la Torre, Biophys. Chem. 93, 159 (2001), Meeting of the British-Biophysical-Society held in Conjunction with the Biochemical-Society, Glasgow, Scotland, 2001.
[42] J. Wohlert, O. Edholm, J. Chem. Phys. 125 (2006) 154905.
[43] J. Kim, S. Ahn, S. Kang, B. Yoon, J. Colloid Interface Sci. 299 (2006) 486.
[44] Y. Solomentsev, Y. Pawar, J. Anderson, J. Colloid Interface Sci. 158 (1993) 1.
[45] S. Allison, Macromolecules 29 (1996) 7391.